

Three-Dimensional Analysis of the Power Transfer Between Crossed Laser Beams

The indirect-drive approach to inertial confinement fusion¹ involves laser beams that overlap as they enter the hohlraum. Because a power transfer between the beams affects the implosion symmetry adversely, it is important to understand the mechanisms that make such a power transfer possible.

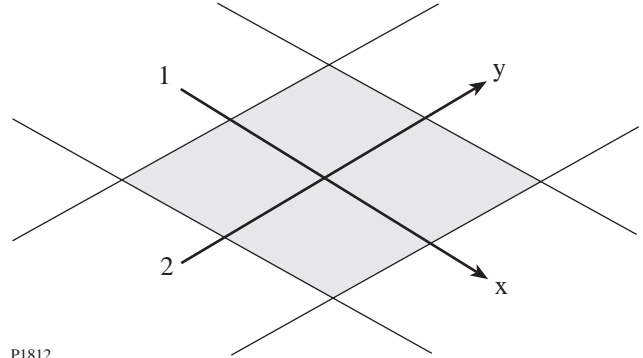
The power transfer between crossed laser beams made possible by an ion-acoustic (sound) wave (grating) has been studied theoretically²⁻⁵ and experimentally.^{6,7} Previously,⁴ we made a two-dimensional analysis of the power transfer between beams with top-hat intensity profiles in a homogeneous plasma. In this article we extend our previous analysis to include three dimensions and arbitrary intensity profiles.

The interaction geometry is illustrated in Fig. 73.34. Notice that the beam axes intersect at the origin. It was shown in Ref. 4 that the steady-state interaction of the beams is governed by

$$\begin{aligned}\partial_x A_1 &= (i\alpha_1 - \beta_1) |A_2|^2 A_1, \\ \partial_y A_2 &= (i\alpha_2 + \beta_2) |A_1|^2 A_2,\end{aligned}\quad (1)$$

where the characteristic variables x and y measure distance in the propagation directions of beams 1 and 2, respectively. The beam amplitude $A_j = (u_j/c_s)(m_e/m_i)^{1/2}$ is the quiver velocity of electrons in the high-frequency electric field of beam j divided by a speed that is of the order of the electron thermal speed. The nonlinear coefficients

$$\begin{aligned}\alpha_j &= \frac{\omega_e^2 \omega_s^2 (\omega_s^2 - \omega^2)}{2\omega_j v_j [(\omega_s^2 - \omega^2)^2 + 4v_s^2 \omega^2]}, \\ \beta_j &= \frac{\omega_e^2 \omega v_s \omega}{\omega_j v_j [(\omega_s^2 - \omega^2)^2 + 4v_s^2 \omega^2]},\end{aligned}\quad (2)$$



P1812

Figure 73.34

Geometry of the interaction of crossed laser beams. The characteristic coordinates x and y measure distance in the propagation directions of beams 1 and 2, respectively.

where ω_j is the frequency of beam j , v_j is the group speed of beam j , $\omega = \omega_1 - \omega_2$ is the difference between the beam frequencies, and $\omega_s = c_s |\mathbf{k}_1 - \mathbf{k}_2|$ and v_s are the sound frequency and damping rate, respectively. Since $|\omega| \ll \omega_1$, the differences between ω_1 and ω_2 , and v_1 and v_2 , can be neglected in Eqs. (2). Henceforth, the subscripts on the nonlinear coefficients will be omitted. These coefficients characterize the way in which the grating responds to the low-frequency ponderomotive force. Apart from a factor of $|A_1|^2$, at resonance β is the spatial growth rate of stimulated Brillouin scattering (SBS) in the strong-damping limit.

It follows from Eqs. (1) that the beam intensities $I_j = |A_j|^2$ satisfy the equations

$$\partial_x I_1 = -2\beta I_2 I_1, \quad \partial_y I_2 = 2\beta I_1 I_2. \quad (3)$$

The boundary conditions are

$$I_1(-\infty, y, z) = J_1(y, z), \quad I_2(x, -\infty, z) = J_2(x, z), \quad (4)$$

where $J_1(y, z)$ and $J_2(x, z)$ are the upstream intensity profiles of the beams.

It follows from Eqs. (3) that the beam evolution in any characteristic plane, labeled by the associated value of z , is independent of the beam evolution in the neighboring planes. Consequently, the method used in Ref. 4 to analyze the two-dimensional interaction of the beam applies, with minor modifications, to the three-dimensional interaction considered herein. This method was used by several authors⁸⁻¹⁰ to study the interaction of two pulses in one spatial dimension and time.

It is convenient to define

$$\begin{aligned} P_1(x, y, z) &= \int_{-\infty}^y I_1(x, y', z) dy', \\ P_2(x, y, z) &= \int_{-\infty}^x I_2(x', y, z) dx'. \end{aligned} \quad (5)$$

Physically, $P_1(x, \infty, z)$ is the power per unit height in the slice of beam 1 that is a distance x from the center the interaction region, and $P_2(\infty, y, z)$ is the power per unit height in the slice of beam 2 that is a distance y from the center of the interaction region. By combining Eqs. (3) and (5), one can show that

$$\partial_x P_1 = J_2 [1 - \exp(2\beta P_1)]. \quad (6)$$

It follows from Eq. (6) that

$$2\beta P_1 = -\log \left\{ 1 - \exp(-\xi) [1 - \exp(-\eta)] \right\}, \quad (7)$$

where the distance variables

$$\xi = 2\beta \int_{-\infty}^x J_2(x', z) dx', \quad \eta = 2\beta \int_{-\infty}^y J_1(y', z) dy'. \quad (8)$$

It follows from Eq. (7), and the relations $I_1 = \partial_y P_1$ and $I_2 = J_2 \exp(2\beta P_1)$, that

$$I_1 = \frac{J_1 \exp(-\eta)}{\exp(\xi) - 1 + \exp(-\eta)}, \quad (9)$$

$$I_2 = \frac{J_2 \exp(\xi)}{\exp(\xi) - 1 + \exp(-\eta)}.$$

By combining Eqs. (3) and (5), one can also show that

$$2\beta P_2 = \log \left\{ 1 + \exp(\eta) [\exp(\xi) - 1] \right\}. \quad (10)$$

Equation (10) and the relations $I_2 = \partial_x P_2$ and $I_1 = J_1 \exp(-2\beta P_2)$ are consistent with solutions (9).

It follows from Eqs. (7) and (10) that

$$P_2(x, y, z) - P_2(x, -\infty, z) = P_1(-\infty, y, z) - P_1(x, y, z), \quad (11)$$

which reflects the fact that the power gained by beam 2 must equal the power lost by beam 1. The power transfer for each slice, $T(z) = P_2(\infty, \infty, z) - P_2(\infty, -\infty, z)$, is given by

$$2\beta T = \log \left\{ \exp(-w_2) + \exp(w_1) [1 - \exp(-w_2)] \right\}, \quad (12)$$

where $w_1(z) = \eta(\infty, z)$ and $w_2(z) = \xi(\infty, z)$ are the normalized beam widths.

When $\alpha \neq 0$, the interaction of beams 1 and 2 causes their phases to be shifted by ϕ_1 and ϕ_2 , respectively. By modifying the analysis of Ref. 4, one can show that the downstream phase shifts

$$\phi_1(y, z) = \alpha P_2(\infty, y, z), \quad \phi_2(x, z) = \alpha P_1(x, \infty, z). \quad (13)$$

According to the laws of geometric optics, the beams are deflected in the direction of increasing phase shift.

Equations (9), (12), and (13) are valid for arbitrary upstream intensity profiles. In the following examples we consider three different profiles: The first profile, $I(u, v) = \exp(-u^2 - v^2)$, is Gaussian, as illustrated in Fig. 73.35(a). The second profile, $I(u, v) = \exp(-u^2 - v^2) \cos^2(\pi u) \cos^2(\pi v)$, has hot spots with a central maximum, as illustrated in Fig. 73.35(b). The third profile, $I(u, v) = \exp(-u^2 - v^2) \sin^2(\pi u) \sin^2(\pi v)$, has hot spots with a central minimum, as illustrated in Fig. 73.35(c). In Figs. 73.36–73.41 all intensities are normalized to I , the peak upstream intensity of a Gaussian beam; all distances are normalized to $1/2\beta I$, the SBS gain length; and all phase shifts are normalized to $\alpha/2\beta$.

In the first example the upstream intensity profiles $I_1(y, z) = \exp(-y^2 - z^2)$ and $I_2(x, z) = 0.5 \exp(-x^2 - z^2)$ are Gaussian. Contour plots of the downstream intensity profiles of beams 1 and 2 are displayed in Figs. 73.36(a) and 73.36(b), respectively. The downstream intensity of beam 2, which has a maximum of 1.2, is higher than the upstream intensity of beam 1. Both beams are distorted by the interaction. Beam 2 grows as it propagates in the positive y direction. Consequently, more power is siphoned from the $y > 0$ side of

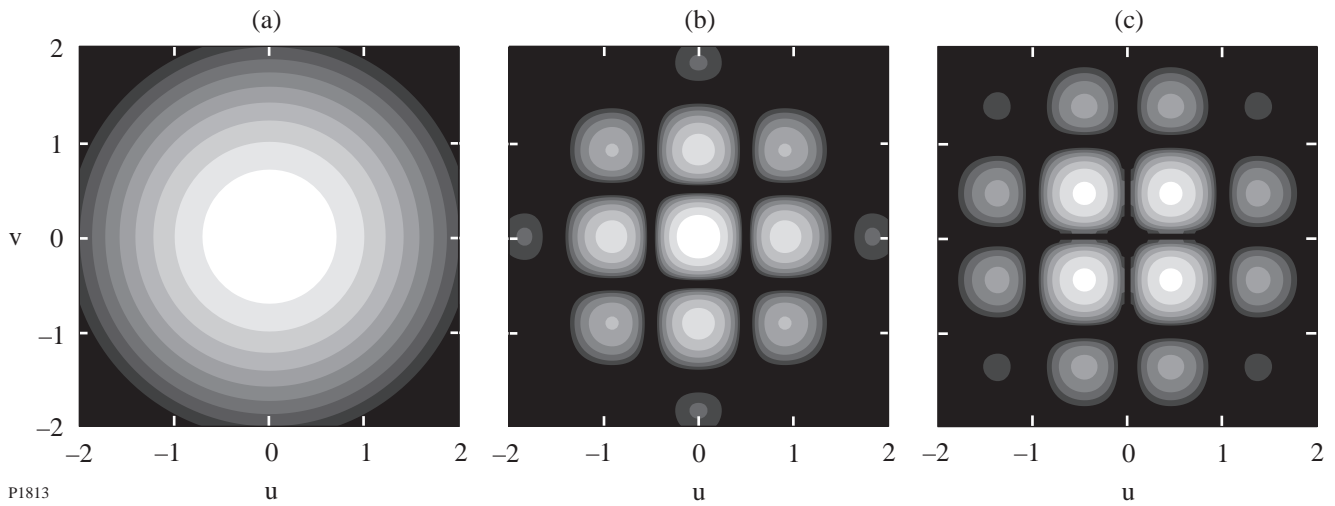
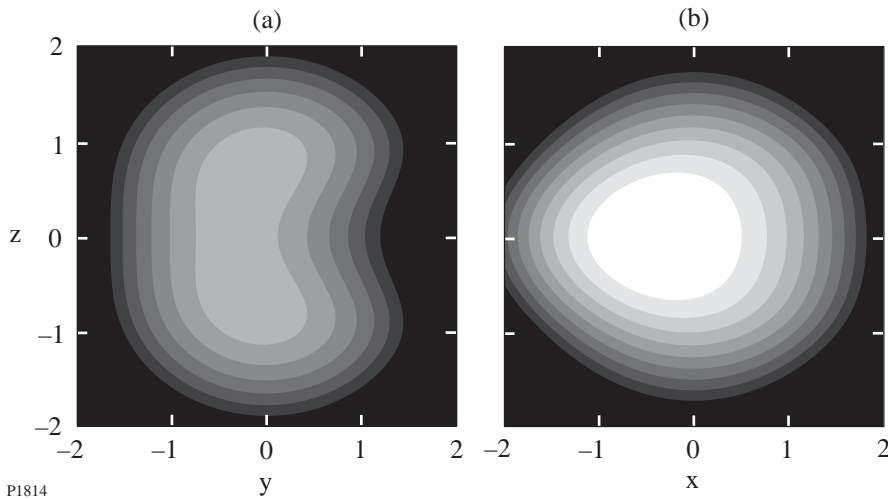
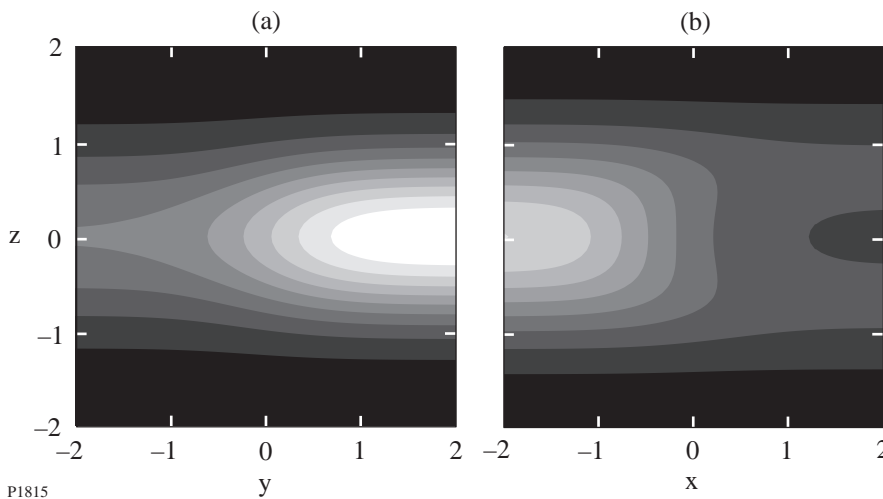


Figure 73.35
 Logarithmic contour plots of the upstream intensity profiles used to generate Figs. 73.36–73.41. White represents high intensity; black represents low intensity. (a) Gaussian profile; (b) profile with hot spots and a central maximum; (c) profile with hot spots and a central minimum.



P1814

Figure 73.36
 Logarithmic contour plots of the downstream intensity profiles of (a) beam 1 and (b) beam 2 corresponding to upstream intensity profiles that are Gaussian. White represents high intensity; black represents low intensity. Both beams are distorted by the interaction, and their centroids are shifted.



P1815

Figure 73.37
 Linear contour plots of the downstream phase shifts of (a) beam 1 and (b) beam 2 corresponding to upstream intensity profiles that are Gaussian. White represents a large positive phase shift; gray represents a small positive phase shift; and black represents a phase shift of zero. Since the beams are deflected in the direction of increasing phase shift, beam 1 is deflected in the positive y direction and beam 2 is deflected in the negative x direction. The upper and lower parts of both beams are deflected toward the z axis.

beam 1 than from the $y < 0$ side, and the centroid of beam 1 is shifted in the negative y direction. The downstream intensity of beam 1 has off-axis maxima because the on-axis slice of beam 1 drives the interaction with the corresponding slice of beam 2 most strongly and is depleted most severely. Beam 1 is depleted as it propagates in the positive x direction. The centroid of beam 2 is shifted in the negative x direction because more power can be siphoned from the undepleted parts of beam 1 than from the depleted parts. Contour plots of the downstream phase shifts of beams 1 and 2 are displayed in Figs. 73.37(a) and 73.37(b), respectively. The maximal phase shift of beam 1 is 2.2. Since the beams are deflected in the direction of increasing phase shift, beam 1 is deflected in the positive y direction and beam 2 is deflected in the negative x direction ($\alpha > 0$). The upper and lower parts of both beams are deflected toward the z axis ($\alpha > 0$).

In the second example the upstream intensity profiles $I_1(y,z) = 4 \exp(-y^2 - z^2) \cos^2(\pi y) \cos^2(\pi z)$ and $I_2(x,z) = 2 \exp(-x^2 - z^2) \cos^2(\pi x) \cos^2(\pi z)$ produce intersecting filaments. The factors of 4 were included to make the beam powers in this example approximately equal to the beam powers in the first example. Contour plots of the downstream intensity profiles of beams 1 and 2 are displayed in Figs. 73.38(a) and 73.38(b), respectively. The maximal intensity of beam 2 is 4.6. According to Eqs. (9), the downstream intensities are the products of the upstream intensities and nonlinear transfer functions that depend on the (spatially integrated) power per unit height of each slice. Thus, the intensity profiles in this example evolve in a manner similar to those in the first example: The centroid of beam 1 is shifted in the negative y direction, and the centroid of beam 2 is shifted in the negative x direction. In this example, however, the

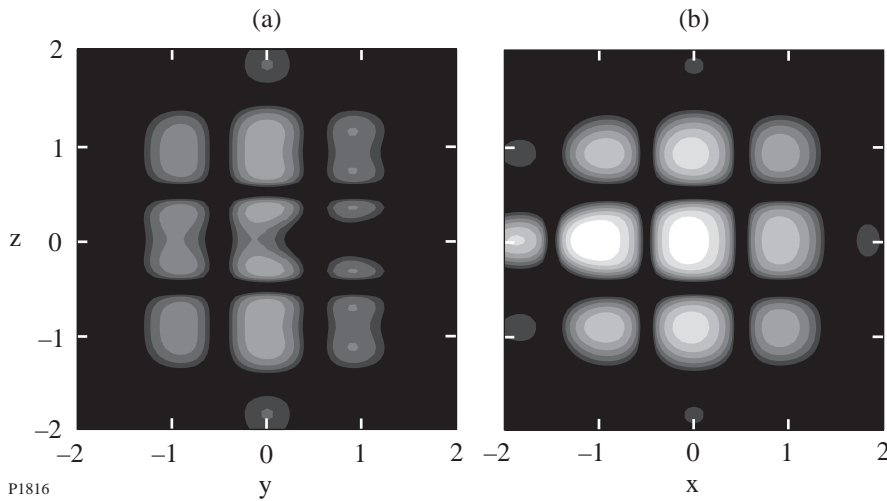


Figure 73.38
Logarithmic contour plots of the downstream intensity profiles of (a) beam 1 and (b) beam 2 corresponding to upstream intensity profiles that produce intersecting filaments. White represents high intensity; black represents low intensity. The beam distortions are more pronounced in this figure than in Fig. 73.36 because the hot-spot intensities are higher than the corresponding intensities of Gaussian beams.

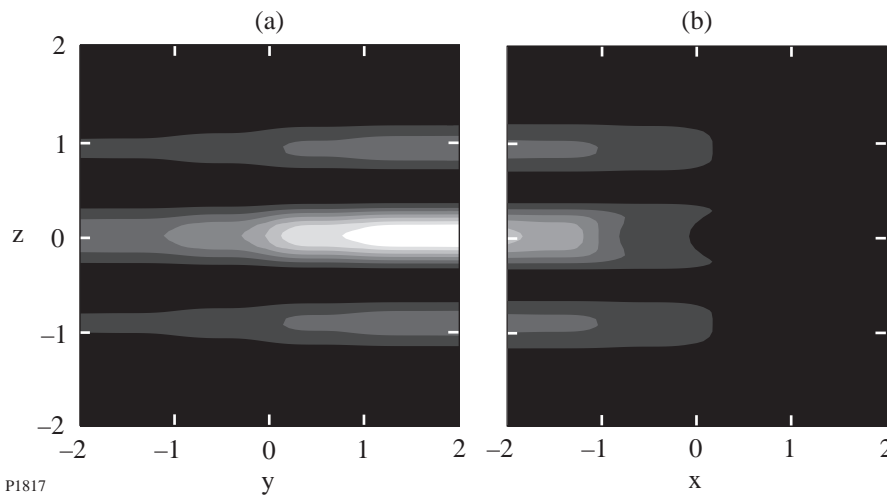


Figure 73.39
Linear contour plots of the downstream phase shifts of (a) beam 1 and (b) beam 2 corresponding to upstream intensity profiles that produce intersecting filaments. White represents a large positive phase shift; gray represents a small positive phase shift; and black represents a phase shift of zero. Beam 1 is deflected in the positive y direction, and beam 2 is deflected in the negative x direction. The upper and lower parts of each row of hot spots are deflected toward the center of the row.

distortions are more pronounced because some slices contain twice the power per unit height of the corresponding slices in the first example. Contour plots of the downstream phase shifts of beams 1 and 2 are displayed in Figs. 73.39(a) and 73.39(b), respectively. The maximal phase shift of beam 1 is 5.1. Beam 1 is deflected in the positive y direction, and beam 2 is deflected in the negative x direction ($\alpha > 0$). The upper and lower parts of each row of hot spots are deflected toward the center of the row ($\alpha > 0$).

In the third example the upstream intensity profiles $I_1(y,z) = 4 \exp(-y^2 - z^2) \cos^2(\pi y) \cos^2(\pi z)$ and $I_2(y,x) = 2 \exp(-x^2 - z^2) \sin^2(\pi x) \sin^2(\pi z)$ produce nonintersecting filaments. Contour plots of the downstream intensity profiles of beams 1 and 2 are displayed in Figs. 73.40(a) and 73.40(b), respectively. The maximal intensity of beam 2 is 2.6. The distortions of the intensity profiles in this example are similar to those in the first and second examples. They are less pronounced, however, because the upstream intensity profiles

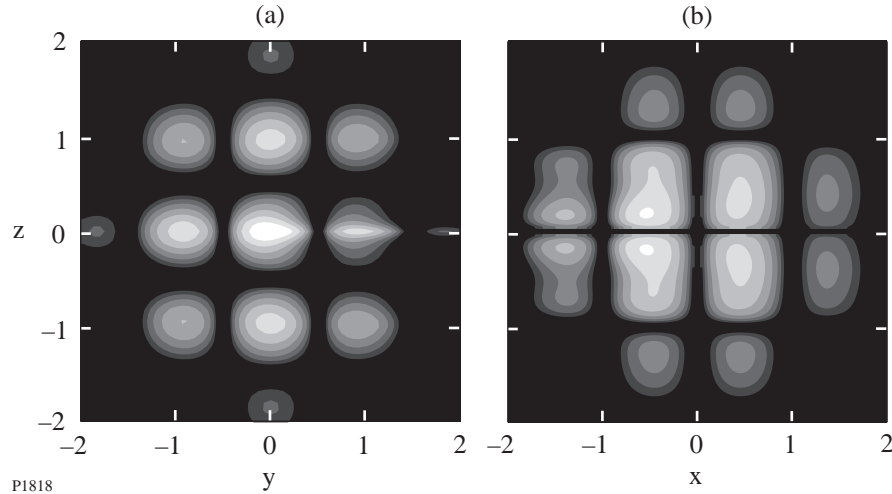


Figure 73.40
Logarithmic contour plots of the downstream intensity profiles of (a) beam 1 and (b) beam 2 corresponding to upstream intensity profiles that produce nonintersecting filaments. White represents high intensity; black represents low intensity. The beam distortions are less pronounced in this figure than in Fig. 73.36 because the beam filaments do not interact strongly.

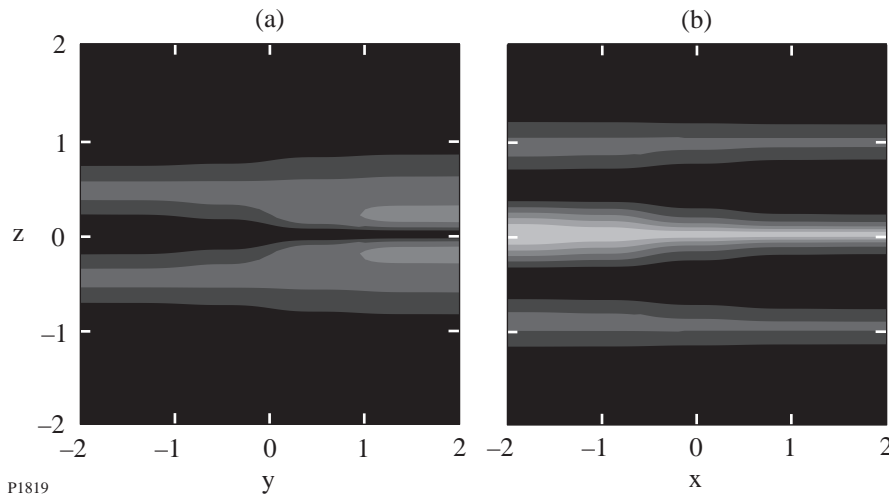


Figure 73.41
Linear contour plots of the downstream phase shifts of (a) beam 1 and (b) beam 2 corresponding to upstream intensity profiles that produce nonintersecting filaments. White represents a large positive phase shift; gray represents a small positive phase shift; and black represents a phase shift of zero. The beam deflections associated with this figure are less important than those associated with Fig. 73.39 because the regions of large phase shift are aligned with the regions of low intensity.

produce filaments that do not interact strongly. Contour plots of the downstream phase shifts of beams 1 and 2 are displayed in Figs. 73.41(a) and 73.41(b), respectively. The maximal phase shift of beam 1 is 2.1. According to Eqs. (13), each beam acquires a phase shift that reflects the intensity profile of the other beam. The regions of large phase shift, however, are aligned with the regions of low intensity, and beam deflections are less important in this example than in the first and second examples.

In summary, we made a three-dimensional analysis of the power transfer between crossed laser beams with arbitrary upstream intensity profiles. We derived simple formulas for the downstream intensity profiles [Eqs. (9)], the power transfer [Eq. (12)], and the downstream phase shifts that depend on the power transfer [Eqs. (13)]. The power transfer shifts the beam centroids, and the phase shifts alter the beam directions and focal lengths. For beams with hot spots in their upstream intensity profiles, the power transfer depends sensitively on whether the associated filaments intersect.

ACKNOWLEDGMENT

This work was supported by the National Science Foundation under Contract No. PHY-9415583, the United States Department of Energy (DOE) under Contract No. W-7405-ENG-36, the U.S. Department of Energy Office of Inertial Confinement Fusion under Cooperative Agreement No. DE-FC03-92SF19460, the University of Rochester, and the New York State Energy Research and Development Authority. The support of DOE does not constitute an endorsement by DOE of the views expressed in this article.

REFERENCES

1. J. D. Lindl, *Phys. Plasmas* **2**, 3933 (1995).
2. W. L. Kruer *et al.*, *Phys. Plasmas* **3**, 382 (1996).
3. V. V. Eliseev *et al.*, *Phys. Plasmas* **3**, 2215 (1996).
4. C. J. McKinstrie, J. S. Li, R. E. Giacone, and H. X. Vu, *Phys. Plasmas* **3**, 2686 (1996). Equations (3) and (4) of this paper were misstated. They should be $A_h = A_1 \exp [i(\mathbf{k}_1 \cdot \mathbf{r} - \omega_1 t)] + A_2 \exp [i(\mathbf{k}_2 \cdot \mathbf{r} - \omega_2 t)] + c.c.$ and $n_l = n \exp [i(\mathbf{k}_1 - \mathbf{k}_2) \cdot \mathbf{r}] + c.c.$, respectively. Equations (5) and (6) are correct.
5. C. J. McKinstrie, V. A. Smalyuk, R. E. Giacone, and H. X. Vu, *Phys. Rev. E* **55**, 2044 (1997).
6. R. K. Kirkwood *et al.*, *Phys. Rev. Lett.* **76**, 2065 (1996).
7. A. K. Lal, K. A. Marsh, C. E. Clayton, C. Joshi, C. J. McKinstrie, J. S. Li, and T. W. Johnston, *Phys. Rev. Lett.* **78**, 670 (1997).
8. M. Maier, W. Kaiser, and J. A. Giordmaine, *Phys. Rev.* **177**, 580 (1969).
9. B. I. Cohen, *Phys. Fluids* **17**, 496 (1974).
10. F. Y. F. Chu, *Phys. Lett.* **51A**, 129 (1975).